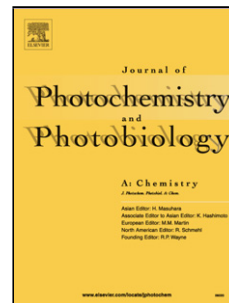# Accepted Manuscript

Title: Highly fluorinated erbium(III) complexes for emission in the C-band

Author: P. Martín-Ramos M. Ramos-Silva F. Lahoz I.R. Martín P. Chamorro-Posada M.E.S. Eusebio V. Lavín J. Martín-Gil

Please cite this article as: P. Martín-Ramos, M. Ramos-Silva, F. Lahoz, I.R. Martín, P. Chamorro-Posada, M.E.S. Eusebio, V. Lavín, J. Martín-Gil, Highly fluorinated erbium(III) complexes for emission in the C-band, *Journal of Photochemistry and Photobiology A: Chemistry* (2014), http://dx.doi.org/10.1016/j.jphotochem.2014.07.008

# Highly fluorinated erbium(III) complexes for emission in the C-band

P. Martín-Ramos[a,b,*], M. Ramos-Silva[b], F. Lahoz[c], I.R. Martín[c], P. Chamorro-Posada[d], M.E.S. Eusebio[e], V. Lavín[c], J. Martín-Gil[a]

[a]  Advanced Materials Laboratory, ETSIIAA, Universidad de Valladolid, Avenida de Madrid 44, 34004 Palencia, Spain. Tel: +34979108347; E-mail: pablomartinramos@gmail.com
[b]  CEMDRX, Physics Department, Universidade de Coimbra, Rua Larga, P-3004-516 Coimbra, Portugal.
[c]  Department of Physics and MALTA Consolider Team, Universidad de La Laguna, E-38200 San Cristóbal de La Laguna, Santa Cruz de Tenerife, Spain.
[d]  Signal Theory and Communications and IT Department, ETSIT, Universidad de Valladolid, Campus Miguel Delibes, Paseo Belén 15, 47011, Valladolid, Spain.
[e]  Chemistry Department, Faculdade de Ciências e Tecnologia, Universidade de Coimbra, P-3004-535 Coimbra, Portugal.

**Abstract.** Two highly fluorinated $Er^{3+}$ complexes with three 6,6,7,7,8,8,8-heptafluoro-2,2-dimethyl-3,5-octanedionate (fod) groups and either bipyridine (bipy) or bathophenantholine (bath) as the ancillary ligand emitting at the C-band (third communication window for fiber transmission) are presented. These complexes are the result of a design process aimed at decreasing the vibrational quenching from high frequency oscillators. The structure of [Er(fod)₃(bipy)] has been elucidated by single-crystal X-ray diffraction, while Sparkle/PM6 and Sparkle/PM7 semi-empirical calculations have been used to model the ground state geometry for [Er(fod)₃(bath)]. Photoluminescence studies confirm sensitization of the $Er^{3+}$ ions by *antenna effect*, leading to NIR emission at 1.53 μm. This energy transfer proves to be more efficient for [Er(fod)₃(bath)] as a result of the bulkier and more rigid structure of bath diimide. The good thermal stability of the materials up to over 200 ºC allows envisaging their use in erbium-doped waveguides, NIR-OLEDs or other optoelectronic devices.

**Keywords**: erbium(III), *β*-diketonate, fluorination, near-infrared, C-band

## 1. Introduction

Long-haul telecommunications depend on fiber-optic networks, which require amplification of the optical signals by using erbium-doped fiber amplifiers (EDFAs) that operate in the 1530-1565 nm wavelength range, the so-called C-band or third window of silica fibers. Since lanthanide ions suffer from low molar absorption coefficients ($\varepsilon$ < 10 L·mol⁻¹·cm⁻¹), the properties of such EDFAs can -in principle- be enhanced by resourcing to photosensitization by conjugated organic species, that is, by incorporating $Er^{3+}$ ions into organic hosts containing chromophores that couple to the $Er^{3+}$ ions, allowing for pumping with lower intensity sources, such as light-emitting diodes (LEDs) and amplification in much shorter lengths [1].

Aforementioned sensitization is attained by the so-called "*antenna-effect*", a term coined by Lehn [2], which denotes the absorption, energy transfer and emission sequence involving distinct absorbing (the ligand) and emitting (the lanthanide ion) components in luminescent lanthanide complexes which work as light conversion molecular devices (LMCDs). This two-step excitation process allows one to achieve a large excited-state population using light fluences (J/cm²) four to five orders of magnitude lower than those required for bare ions [3,4].

However, in particular case of $Er^{3+}$ ion, because of the relatively small energy gap between the $^4I_{13/2}$ excited state and the $^4I_{15/2}$ ground state, the excited state is efficiently quenched by the vibronic coupling with high energy O–H and C–H stretching vibrations in the neighborhood of the $Er^{3+}$ ion, originated from the ligands, polymer matrix or solvents. Consequently, in order to improve overall quantum yields, excluding hydrogen atoms from the lanthanide ion

1

surroundings (>20 Å) [5] should be regarded as an essential requirement for the design of $Er^{3+}$ chromophores, in addition to the usual considerations aimed at achieving high sensitization efficiencies. This requirement can be achieved by (i) preventing solvent molecules from entering in the lanthanide first coordination sphere and (ii) by using ligands with low hydrogen content.

The removal of solvent molecules can be efficiently achieved by the use of N,N-donor molecules: these ligands act as Lewis bases, and form adducts with tris $\beta$-diketonate complexes because of the tendency of the lanthanide ion to expand its coordination sphere and to achieve a coordination number higher than six (typically eight or nine). On the other hand, deuteration and halogenation of the ligands (i.e., the substitution of H atoms in the aromatic rings with halogens atoms such as fluorine [6-8], chlorine [9] and bromine [10]) has proven to be a successful approach for the second objective. Absorptions are diminished (C-D) or absent (C-F), because the third overtone of C-D is located at 1.5 µm and the third overtone of C-F at 2.6 µm.

In an attempt to simultaneously fulfill both requirements, we have designed two highly fluorinated erbium(III) complexes, with general formula $[Er(fod)_3(N,N-donor)]$, where fod corresponds to 6,6,7,7,8,8,8-heptafluoro-2,2-dimethyl-3,5-octanedionate and N,N-donor is either bipyridine (bipy) or bathophenantholine (bath): the introduction of N,N-donor molecules in the coordination sphere of $Er^{3+}$ excludes the effect of O-H oscillators and the use of a perfluorinated ligand (Hfod) minimizes the deleterious effect of C-H oscillators. In this article, we report their synthesis, structural elucidation by single crystal X-ray diffraction and semi-empirical quantum chemistry calculations, and a thorough characterization by X-ray powder diffraction (XRPD), NMR, ATR-FTIR and Raman spectroscopies, DSC, absorption and photoluminescence studies.

## 2. Experimental

### 2.1. *Materials, synthesis and analytical data*

All reagents and solvents employed were commercially available and used as supplied without further purification. All the procedures for complex preparation were carried out under nitrogen and using dry reagents to avoid the presence of water and oxygen, which can quench metal luminescence.

Tris(6,6,7,7,8,8,8-heptafluoro-2,2-dimethyl-3,5-octanedionate)mono(2,2'-bipyridine) erbium(III), $[Er(fod)_3(bipy)]$, was obtained as follows: under stirring, a Hfod (3 mmol) methanol solution (20 ml) was added to a 1 mmol of $Er(NO_3)\cdot 5H_2O$ in methanol. The mixture was neutralized by adding potassium methoxide (3 mmol) dropwise under vigorous stirring until potassium nitrate precipitated. $KNO_3$ was removed by decanting, and 2,2'-bipyridine (1 mmol) was finally added. The mixture was heated to 75 ºC and stirred overnight, then washed with dioxane, and lastly dried in vacuum to give product in 95% yield (based in $Er^{3+}$). Crystals suitable for X-ray analysis were obtained by slow evaporation of a methanol-dioxane solution at room temperature (RT).

The synthesis procedure for $[Er(fod)_3(bath)]$ is analogous, using 1 mmol of bathophenanthroline instead of 2,2'-bipyridine.

$[Er(fod)_3(bipy)]$: Chemical formula: $C_{40}H_{38}ErF_{21}N_2O_6$. $M_W$: 1208.96. Anal. Calcd. for $C_{40}H_{38}ErF_{21}N_2O_6$: C, 39.74; H, 3.17; Er, 13.83; F, 33.00; N, 2.32; O, 7.94. Found: C, 39.76; H, 3.16; N, 2.38.

$[Er(fod)_3(bath)]$: Chemical formula: $C_{54}H_{46}ErF_{21}N_2O_6$. $M_W$: 1385.18. Anal. Calcd. for $C_{54}H_{46}ErF_{21}N_2O_6$: C, 46.82; H, 3.35; Er, 12.07; F, 28.80; N, 2.02; O, 6.93. Found: C, 46.71; H, 3.29; N, 2.05.

2

**2.2.**

### 2.3. *X-ray crystallographic analysis*

The crystal structures were investigated by X-ray diffraction analysis. Prior to structural characterization, the powder diffractograms of the erbium complexes were recorded using a Bruker D8 Advance Bragg-Brentano diffractometer, in reflection geometry. For the determination of crystal structures by X-ray diffraction, single crystals of the complexes were glued to glass fibres and mounted on a Bruker APEX II diffractometer. Diffraction data was collected at room temperature 293(2) K using graphite monochromated MoKα (λ=0.71073 Å). Absorption corrections were made using SADABS [11]. [Er(fod)$_3$(bipy)] structure was solved by direct methods using SHELXS-97 [12] and refined anisotropically (non-H atoms) by full-matrix least-squares on $F^2$ using the SHELXL-97 program [12]. [Er(fod)$_3$(bath)] structure was partially solved: the lanthanide ions, the bathophenanthroline and the middle diketonate portion of the fluorinated ions could be located. The remaining atomic positions could not be reliably found, due to the low resolution of the difference Fourier map (very large unit cell, two independent complexes). This partial model refined on $F^2$ yielded an $R$=16%. PLATON [13] was used to analyse the structure, for figure plotting and for powder diffractogram simulations.

### 2.4. *Computational procedure*

The crystal parameters and part of the structure of [Er(fod)$_3$bath)] complex were determined from X-Ray data. The initially known data included, apart from the position of the 16 Er$^{3+}$ ions, all the atoms in their first coordination spheres, the aromatic section of the fod ligands and the entire bathophenanthroline unit. The rest of the complex geometry (namely the rest of the fod chain) was optimized using semiempirical methods for each complex in the unit cell. The computations were performed using the MOPAC2012 software [14,15] parallel version based on OpenMPI using the SPARKLE/PM7 [16,17] and the SPARKLE/PM6 Hamiltonians [18,19] on a server with four AMD Opteron 16 Core processors and 128 GB of memory and a Linux operating system.

The calculations have been run both for the standalone molecule, with crystal symmetry imposed, and for the entire unit cell, which consists of a total 2080 atoms. In the later case, periodic boundary conditions have been used by using the keyword MERS=(1,1,1). Initially, only the unknown part of the crystal was optimized, while all the known part of the complex geometries were kept fixed in the optimization process.

For the standalone molecule, the default convergence at a gradient norm below 1 kcal/mol/Ansgrom was obtained both for the PM6 and PM7 Hamiltonians. For the entire unit cell, a convergence down to 13.192 kcal/mol/Angstrom gradient norm was initially obtained with the PM6 Hamiltonian and 9.562 kcal/mol/Angstrom for the PM7 Hamiltonian. The geometry obtained was subsequently used as the initial data for a second geometry optimization where only the position of the Er$^{3+}$ atoms and the crystal cell parameters were kept fixed. In this case, convergence was obtained down to 11.230 kcal/mol/Angstrom for the PM6 Hamiltonian and to 7.596 kcal/mol/Angstrom for the PM7 Hamiltonian.

### 2.5. *Physical and spectroscopic measurements*

The C, H, N elemental analyses were conducted using a Perkin Elmer CHN 2400 apparatus. Differential scanning calorimetry (DSC) data were obtained on a DSC Pyris1 Perkin Elmer instrument, equipped with an intracooler cooling unit at -25 ºC (ethylenglycol-water, 1:1 v/v, cooling mixture), with a heating rate $\beta$=10°C/min, under a N$_2$ purge, 20 mL/min.

Infrared spectra were recorded with a Thermo Nicolet 380 FT-IR apparatus equipped with Smart Orbit Diamond ATR system. Raman spectra were recorded with a FT-Raman Bruker FRA106 by using a near-IR (Nd: YAG, 1064.1 nm) laser to excite the sample. $^1$H-NMR spectra were registered from deuterated chloroform solution (CDCl$_3$) using a 400 MHz NMR

3

spectrometer from Varian Mercury 400 (9.4 T) at 400.123 MHz. ^{13}C-NMR and ^{19}F-NMR spectra were recorded at 100.6 and 376.5 MHz, respectively.

The optical absorption and diffuse reflectance of the materials were measured at room temperature in solution and in powder, respectively: the 200-800 nm range absorption spectra were recorded with a spectrophotometer (Hitachi U-2010) in methanol diluted solutions ($10^{-5}$M and $10^{-3}$M), and UV-Vis-NIR diffuse reflectance spectra in the range from 200 to 1800 nm were measured using an integrating sphere coupled to a spectrophotometer (Agilent Cary 5000) in powder form.

The photoluminescence (PL) spectra in the UV-Vis region and the ligand fluorescence decays were obtained using a 280 nm picosecond pulsed light emitting diode (Edinburgh Instruments EPLED-280) with a typical pulse width of 700 ps and a 405 nm picosecond pulsed diode laser (Edinburgh Instruments EPL-405) with a typical pulse width of 80 ps. The emission spectra and the ligand fluorescence decays were recorded using a fluorescence spectrometer with a single photon counting multichannel plate photomultiplier and a dedicated acquisition software (Edinburgh Instruments LifeSpec II and F900 software). The NIR PL spectra were measured exciting the samples using either the 800 nm radiation of a cw Ti:sapphire laser (Spectra Physics 3900S) pumped by a 10 W cw $Ar^+$ laser (Spectra Physics 2060-10 Beamlock) or a 450 W Xenon arc lamp followed by a 0.22 m double-grating monochromator (Spex 1680) to provide an excitation beam centered at 360 nm. The NIR emissions were focused with a convergent lens onto a 0.18 m single-grating monochromator (Jobin Yvon Triax180) with a resolution of 0.5 nm and then detected with an InGaAs detector. The NIR luminescence decay curves were measured upon excitation of the $Er^{3+}$ ions at 980 nm with a Spectra Physics Quanta-Ray MOPO-730 laser system. The emitted light was dispersed using a single-grating 0.34 m focal length spectrometer (Spex 340E) and detected with a Peltier-cooled, NIR-extended photomultiplier (Hamamatsu H9170-75) and a lock-in amplifier. Lifetimes were measured by using a digital oscilloscope (Tektronix TDS520). All spectra were corrected for the spectral response of the equipments.

## 3. Results and discussion

### 3.1. *Crystallographic analysis*

#### 3.1.1. *Structural description*

[Er(fod)$_3$(bipy)] crystallizes in the monoclinic P2$_1$/c with four symmetry-related molecules in each unit cell of volume 4877.1 Å$^3$ (see Figure 1 and Table 1). Each lanthanide ion is coordinated by two nitrogen atoms and six oxygen atoms that constitute the vertices of a square antiprism. The top and bottom faces of the antiprism make an angle of 2.08(9)º and the lanthanide that sits approximately in the centre of the polyhedron is at a distance of 1.3685(1) and 1.2002(1) Å to the top and bottom faces. There are signs of conformational disorder in the fluorinated ligands; the fluorine atoms display large thermal ellipsoids and the -C(CH$_3$) terminal groups could be refined over two positions. The unit cells do not contain any residual solvent accessible voids.

4

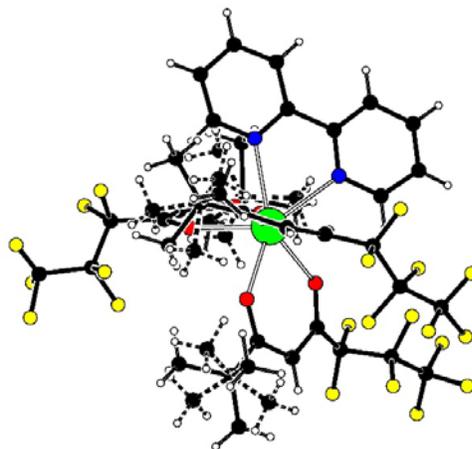**Figure 1.** Structural diagram for [Er(fod)$_3$(bipy)], with O atoms in red, N atoms in blue, F atoms in yellow and Er atoms in green.

[Er(fod)$_3$(bath)] calculated structure is shown in Figure 2. The two symmetry independent complexes exhibit a square-antiprismatic coordination of the Er$^{3+}$ ions in the predicted structures. For PM7, the top and bottom faces make an angle of 3.0º for Er1 [0.45º for Er2] and Er1 is at a distance of 1.363 and 1.146 Å from the top and bottom faces [1.383 and 1.220 Å for Er2].
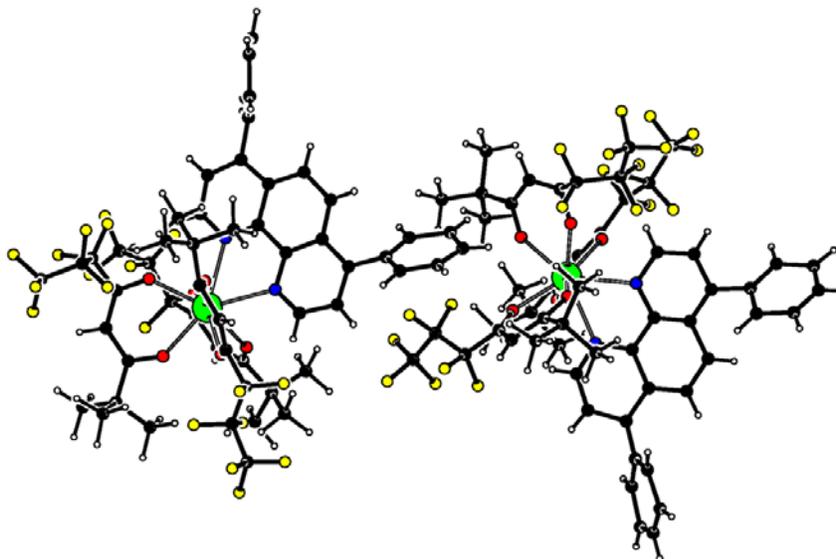


**Figure 2.** Predicted conformation for [Er(fod)$_3$(bath)] using PM7, according to CPK color code.

**Table 1**. Crystal data and structure refinement for the complexes with 6,6,7,7,8,8,8-heptafluoro-2,2-dimethyl-3,5-octanedione

| Complex | [Er(fod)$_3$(bipy)] | [Er(fod)$_3$(bath)] |
|---|---|---|
| Empirical formula | C$_{40}$H$_{38}$ErF$_{21}$N$_2$O$_6$ | C$_{54}$H$_{46}$ErF$_{21}$N$_2$O$_6$ |
| Formula weight | 1208.98 | 1385.18 |
| Temperature (K) | 293(3) | 293(3) |
| Wavelength (Å) | 0.71073 | 0.71073 |

5

| | Monoclinic | Orthorhombic |
|---|---|---|
| Crystal system | Monoclinic | Orthorhombic |
| Space group | $P2_1/c$ | $Pcan$ |
| $a$ (Å) | 13.8124(3) | 25.5335(6) |
| $b$ (Å) | 20.3813(5) | 28.8665(7) |
| $c$ (Å) | 18.1497(5) | 32.5392(8) |
| $\alpha$ (º) | 90.00 | 90.00 |
| $\beta$ (º) | 107.342(2) | 90.00 |
| $\gamma$ (º) | 90.00 | 90.00 |
| Volume (Å$^3$) | 4877.1(2) | 23983.4(10) |
| $Z$ | 4 | 8 |
| Calculated density (g cm$^{-3}$) | 1.647 | |
| Absorption coefficient (mm$^{-1}$) | 1.845 | |
| $F$(000) | 2388 | |
| Crystal size (mm$^3$) | 0.44×0.40×0.08 | |
| θ range for data collection | 1.84-25.77º | |
| Index ranges | -16<$h$<16; -24<$k$<24; -22<$l$<22 | |
| Reflections collected | 97420 | |
| Independent reflections | 6848 | |
| Completeness to 2θ=51º | 0.996 | |
| Refinement method | Full matrix LS on $F^2$ | |
| Data/restrains/parameters | 9310/163/735 | |
| Goodness-of-fit on $F^2$ | 1.034 | |
| Final $R$ indices [$I$>2σ($I$)] | $R$=0.0521; w$R$=0.1442 | |
| $R$ indices (all data) | $R$=0.0741; w$R$=0.1669 | |
| Largest diff. peak and hole | -0.807/1.370 | |

Er-O and Er-N distances for the two complexes are summarized in Table 2. For [Er(fod)$_3$(bipy)], the distances are within normal ranges [20]. With regard to [Er(fod)$_3$(bath)], the values obtained using PM7 Hamiltonian are significantly closer to the experimental average values for [Er($\beta$-diketonate)$_3$(bath)] complexes [2.288 Å for Er-O and 2.554 Å for Er-N] [21-24] than those for PM6 Hamiltonian. This is in agreement with the observations made by Stewart [16]: a significant increase in accuracy has been achieved in PM7 after relatively minor changes were made to the approximations and after proxy reference data functions representing non-covalent interactions were introduced, leading to a reduction of errors in PM7 geometries by over one-third relative to those of PM6.

**Table 2**. Er-N and Er-O distances in Å for the complexes with 6,6,7,7,8,8,8-heptafluoro-2,2-dimethyl-3,5-octanedione

| Bond | [Er(fod)$_3$(bipy)] SC-XRD | [Er(fod)$_3$(bath)] starting model from SC-XRD | [Er(fod)$_3$(bath)] PM6 model | [Er(fod)$_3$(bath)] PM7 model |
|---|---|---|---|---|
| Er-N avg. | 2.523 | 2.520 | 2.370 | 2.467 |
| Er-O avg. | 2.297 | 2.285 | 2.352 | 2.296 |

### 3.1.2. *X-ray powder diffraction*

The experimental diffraction patterns for the two Er$^{3+}$ complexes are shown in Figure 3. For [Er(fod)$_3$(bipy)], the simulated powder pattern obtained from the single crystal structure using PLATON [13] is also shown for comparison. There is an excellent match between the simulated and the experimental diffractograms: the peaks appear at the predicted theta angles. In this case, powder diffraction shows that all the material synthesized contains the same structure as the small single crystals used for single-crystal X-ray diffraction.

For [Er(fod$_3$(bath)] complex, Figure 4 depicts the experimental data, the simulated powder diffractograms with increasing complexity of the structural model using PLATON [13], and the simulated patterns from the ground state geometry using semiempirical calculations (PM6 and PM7 Hamiltonians). As it can be inferred from Figure 4, the simulated diffractogram containing

6

the $Er^{3+}$ ions and the N,O atoms from the first coordination sphere (PLATON sim. 2) accounts well for many of the experimental peaks, with the peak positions agreeing with the experimental ones. The remaining experimental peaks could be explained by Bragg reflections from planes containing mostly the ligand atoms and/or solvent atoms. In fact, the more we complete the model (PLATON sim. 3), the more peaks are predicted and, of course, relative intensities are changed. On the other side, the imperfect agreement of these simulations indicates that the ligand position/orientation is not corresponding to the true average positions. In the solid state, disorder is most likely to occur: similar compounds have shown disorder in the chain conformation, $CF_2$ and $CF_3$ groups, and can even interchange the bulky N,N-donor and a $\beta$-diketonate chain [23,21,25,26].
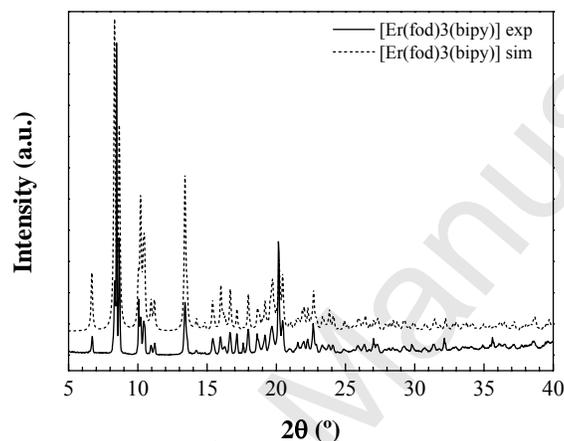


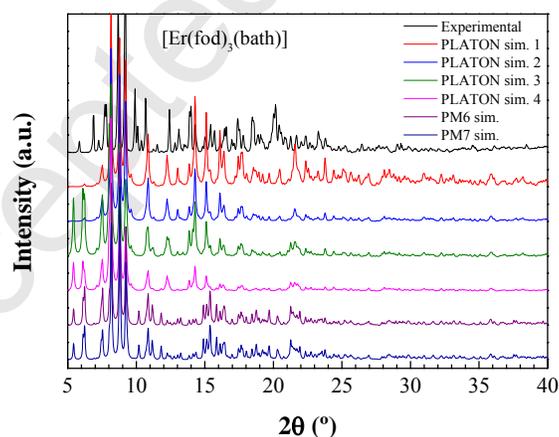**Figure 3.** Experimental and simulated X-ray powder diffraction patterns of [Er(fod)$_3$(bipy)] complex.



**Figure 4.** Experimental and simulated X-ray powder diffraction patterns of [Er(fod)$_3$(bath)] complex. PLATON sim. 1 was obtained considering only the Erbium atoms in the unit cell. For PLATON sim. 2, the model included also the coordinating N and O atoms. In PLATON sim. 3, the bath molecule was added to the model. In PLATON sim. 4, the central part of the $\beta$-diketonate ligands was included in the model (starting point for the PM6 and PM7 calculations). PM6 and PM7 are the simulated diffractograms using the full calculated structural model with PM6 and PM7 Hamiltonians, respectively.

7

**3.2.**

**3.3.** *NMR spectroscopy*

In the particular case of [Er(fod)$_3$(bath)] complex, for which the SC-XRD structure could not be fully resolved, additional structural elucidation data has been recorded by means of NMR spectroscopy measurements.

*$^1$H-NMR*. The $^1$H-NMR spectrum of the [Er(fod)$_3$(bath)] complex (see Figure 5a) displays, apart from a strong signal at 7.24 ppm associated to CDCl$_3$ and a very weak band at 1.68 corresponding to HOD in CDCl$_3$, the following signals associated to the fod $\beta$-diketonate: 0.95 ppm (methyl protons), 1.2 ppm (tert-butyl protons) and 2.5 ppm (carbonyl group). Those at 9.7, 10.2 and 13.3 ppm can be assigned to methine protons [27].

*$^{13}$C-NMR*. Figure 5b shows the $^{13}$C-NMR spectrum of [Er(fod)$_3$(bath)], in which the signal at 77.2 can be assigned to CDCl$_3$. The signal at 26.1 ppm should be assigned to the aliphatic CH$_3$ in fod $\beta$-diketonate, while signals in the 122.9-143.9 ppm region should be referred to 1-ethylene, quinoline and 1-benzene from the bathophenanthroline moiety.

*$^{19}$F-NMR*. The $^{19}$F-NMR spectrum (Figure 5c) displays one strong signal at -78.35 due to –CF$_3$ groups and an additional doublet of medium intensity around -132 ppm assignable to -CF$_2$ groups.
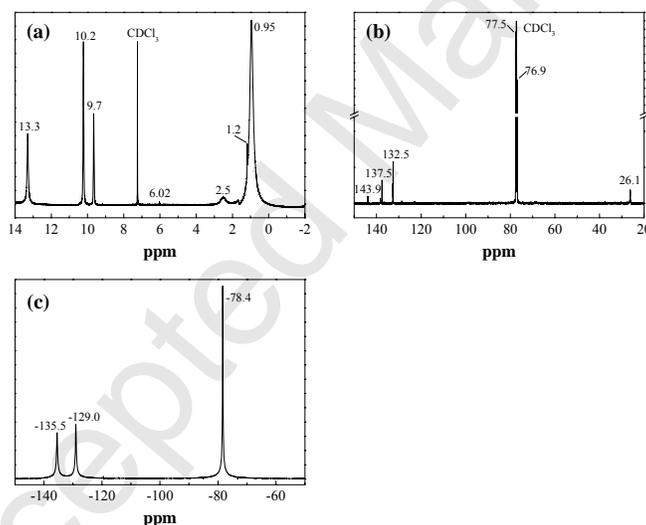


**Figure 5**. (*a*) $^1$H-NMR, (*b*) $^{13}$C-NMR and (*c*) $^{19}$F-NMR spectra for [Er(fod)$_3$(bath)] complex.

**3.4.** *Thermal analysis by DSC*

The DSC curves of these complexes (under N$_2$ atmosphere) show endothermic effects under 150 ºC and exothermic effects above 240 ºC (see Figure 6). Whereas for [Er(fod)$_3$(bath)] complex there is a single endotherm corresponding to melting at 101 ºC, [Er(fod)$_3$(bipy)] shows two separate peaks associated to pre-melting (at 79.5 ºC) and melting (130.1 ºC), respectively. The onset of decomposition/volatilization begins in both samples at ca. 240 ºC, although the process appears to be slower for the bipy than for the bath adduct, with decomposition maxima at around 340 ºC and 280 ºC, respectively.

The stability of the complexes is similar to that of other lanthanide complexes with the same $\beta$-diketonate fod ligand reported by Irfanullah *et al.* [27,28], though in these later the onset of volatilization begins at 215 ºC and evaporation is complete at 325-350 ºC. The lower melting points for the complexes presented herein is attributed to the fact that mononuclear complexes are thermally less stable than their dinuclear analogues [29].
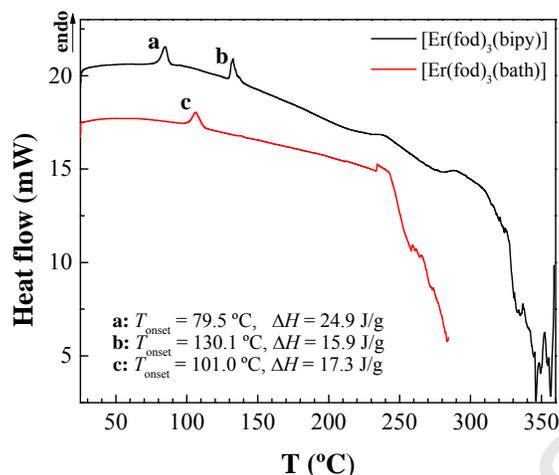
8

**Figure 6.** DSC curves for [Er(fod)$_3$(bipy)] (*black*) and [Er(fod)$_3$(bath)] (*red*).

### 3.5. *Infrared spectroscopy*

The IR absorption spectra for the complexes are shown in Figure 7. The absorption bands have been identified in accordance with the literature [30]: 1645-1653 cm$^{-1}$ ($\nu_{as}$C=C-C=O), 1618-1623 cm$^{-1}$ ($\nu_s$C=C-C=O), 1580 cm$^{-1}$ ($\nu$C=C), 1475 cm$^{-1}$ ($\nu_{as}$C-C=C-O), 1344 cm$^{-1}$ ($\nu_s$C-C=C-O), 1440 cm$^{-1}$ ($\nu_{as}$C=N), 1391 cm$^{-1}$ ($\nu_s$C=N) and 1017–1105 cm$^{-1}$ range (ring 'breathing' modes). They are shifted in comparison with those of the free ligands, suggesting that the fod $\beta$-diketonate ligands and the N,N-donor moieties are coordinated to Er$^{3+}$ ions.

The absorption bands characteristic of the bipy and bath diimides, in the 739-1020 cm$^{-1}$ range, associated to γCH, in-plane ring (phenyl and pyridyl) and CH bendings, provide further evidence that the Er$^{3+}$ ion is coordinated to the ancillary ligands, since they are appreciably red shifted (*vs*. those of free ligands) due to the perturbation induced by the coordination to the lanthanide ion.

An important feature –provided that they are fluorinated complexes– is the occurrence of strong carbon–fluorine bands in the 1116 to 1283 cm$^{-1}$ range, assigned to CF$_3$ as (C–F) stretching modes (*viz.*, νC-CF$_3$ at 1283 and 1218 cm$^{-1}$, $\nu_{as}$CF$_3$ at ca. 1148 cm$^{-1}$ and $\nu_s$CF$_3$ at 1117 cm$^{-1}$). In addition, the bands at around 573 and 629 cm$^{-1}$ can be assigned to δCF$_3$ vibrations [31].

Finally, the low absorption in the region at around 3000 cm$^{-1}$ (attributed to C–H aliphatic and C–H aromatic vibrations) and the absence of absorption at 3500 cm$^{-1}$ (not shown), is the expected for a low amount of CH and OH groups, as planned in the preparative conditions.
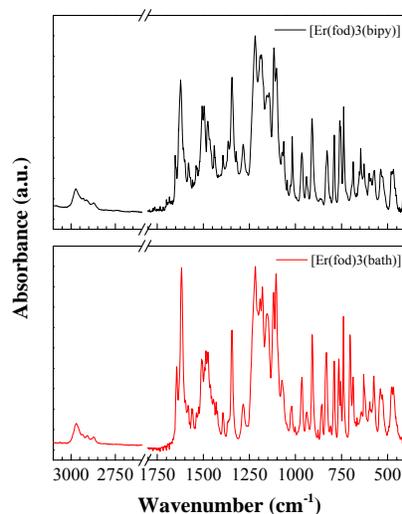
9

**Figure 7**. ATR-FTIR spectra of [Er(fod)$_3$(bipy)] (*top*) and [Er(fod)$_3$(bath)] (*bottom*).

### 3.6. *Raman spectroscopy*

The Raman spectra of the complexes, depicted in Figure 8, show the expected frequencies for the coordinated fod $\beta$-diketonate and N,N-donors. The higher wavenumber bands, in the 1351-1626 cm$^{-1}$ range, can be assigned to C=C, C=O and C=N stretching vibrations, with additional C=C stretching bands at around 1270 cm$^{-1}$ and C=O stretching peaks at ca. 1200 cm$^{-1}$. The peak at around 750 cm$^{-1}$ corresponds to C-H out of plane bending, while that at 650 cm$^{-1}$ is associated to ring deformation modes of bipy and bath.

CF$_3$ associated vibrations appear at ca. 1290 cm$^{-1}$, 1102 cm$^{-1}$ and 1060 cm$^{-1}$.

The bands in the 2800-3085 cm$^{-1}$ region are ascribed to C-H stretching from the non-fluorinated CH$_3$ end of the fod $\beta$-diketonate.

The bands in the lower wavenumber range (below 421 cm$^{-1}$) can be tentatively assigned to $\nu$(Er–O) and $\nu$(Er–N) modes, in agreement with Liang *et al.* [32].
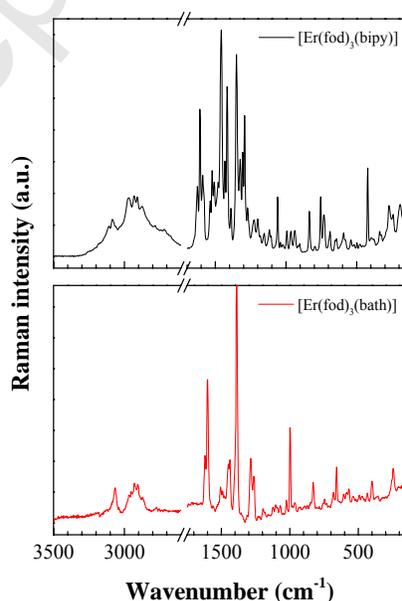


**Figure 8**. Raman spectra of [Er(fod)$_3$(bipy)] (*top*) and [Er(fod)$_3$(bath)] (*bottom*)

10

### 3.7. *Absorption spectra*

The RT spectra derived from absorption and diffuse reflectance measurements of the complexes in the UV-visible-NIR range (200-2000 nm) are shown in Figure 9. The broad and intense absorption bands in the 200-350 nm range are associated to the organic ligands $\pi$-$\pi$* transitions from the $S_0$ ground state to the $S_1$ excited state [33]. They are formed by the overlap of a main band centered at about 270 nm and two other components at ca. 220 and 320 nm. For a better understanding of the UV absorption bands, the UV-Vis (210-800 nm) absorption spectra were also recorded in $10^{-5}$M methanol diluted solutions (see the inset in Figure 9), allowing a more resolved spectra of the ligands absorption. The maxima in this case are at around 285 nm and thus can be assigned to the $\pi \rightarrow \pi$* intra-ligand transition in the fod moiety [34-36]. Consequently, the main peak observed in the solid powder measurements at about 270 nm can be tentatively assigned to electronic intraligand transitions in the fod moiety, while the other components would be due to $\pi \rightarrow \pi$* transitions in the diimide molecules, in agreement with Gerasimova *et al.* [37].

Moreover, sharp peaks associated to intra-configurational $4f^{11}$–$4f^{11}$ electronic transitions starting from the $^4I_{15/2}$ ground state to the different excited levels of the $Er^{3+}$ ion can be discerned. The bands correspond to the transitions from the $^4I_{15/2}$ ground state to $(^4G_{9/2},{}^2K_{15/2},{}^2G_{7/2})$ (~355.5 nm), $^4G_{11/2}$ (376.5 nm), $(^2G,{}^4F,{}^2H)_{9/2}$ (~405 nm), $(^4F_{5/2},{}^4F_{3/2})$ (~449.5 nm), $^4F_{7/2}$ (~486.5 nm), $^2H_{11/2}$ (~522 nm), $^4S_{3/2}$ (~544 nm), $^4F_{9/2}$ (~660 nm), $^4I_{9/2}$ (~802 nm), $^4I_{11/2}$ (~977 nm) and $^4I_{13/2}$ (~1532 nm) $Er^{3+}$ excited states [38]. Figure 9 also shows the second and third overtones of aromatic C–H stretching vibration, which appear near 1675 nm and 1140 nm, respectively. It is worth noting that none of the detected C-H vibration overtones coincides with the NIR emission band of $Er^{3+}$ ions centered at around 1530 nm and, consequently, a quenching of the $Er^{3+}$ NIR luminescence is not expected due to energy transfer to C-H vibrational modes.
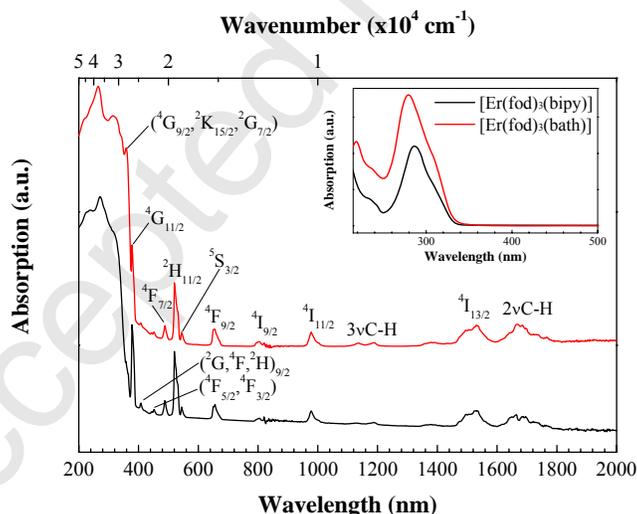


**Figure 9.** Diffuse reflectance spectra of [Er(fod)₃(bipy)] (*black*) and [Er(fod)₃(bath)] (*red*) complexes in the UV-visible-NIR range at RT. All transitions start from the $^4I_{15/2}$ ground state to the indicated levels. An offset in the *y*-axis has been added for clarity reasons. *Inset*: UV-Vis absorption spectra in methanol diluted solutions ($10^{-5}$M) using a quartz cuvette with L=5 cm.

### 3.8. *Excitation spectra and photoluminescence emission*

*PL emission in the visible range.* The emission from the $Er^{3+}$ complexes in the visible region have firstly been studied under direct excitation of the organic ligands with 280 nm LED radiation, in resonance with the $\pi \rightarrow \pi$* intra-ligand transition of the fod moiety. The visible spectra (see Figure 10) feature an intense broad band which peaks at ca. 365 nm for [Er(fod)₃(bipy)] complex and at ca. 400 nm for [Er(fod)₃(bath)] complex. These bands are

11

attributed to $S_0 \rightarrow S_1$ transitions of *β*-diketonate and heterocyclic ligands, with the peak position being related to the specific diimide, in agreement with Irfanullah *et al.* [39,33,29]. On the other hand, the relaxation of the organic parts of these samples can also undergo intersystem crossing (ISC) to the triplet level due to spin reorientation, from which subsequent resonant energy transfer (RET) to $Er^{3+}$ takes place (see Figure 11), as it will be further discussed below.
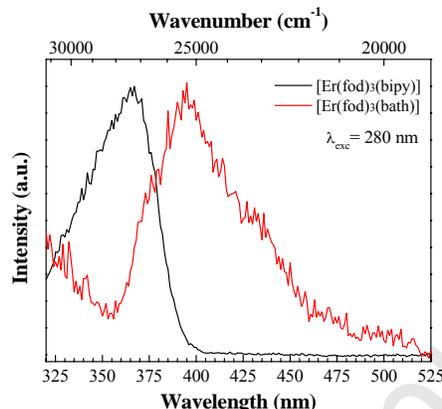


**Figure 10.** Photoluminescence spectra in the visible region for the [Er(fod)$_3$(bipy)] (*black*) and [Er(fod)$_3$(bath)] (*red*) complexes upon excitation at 280 nm.
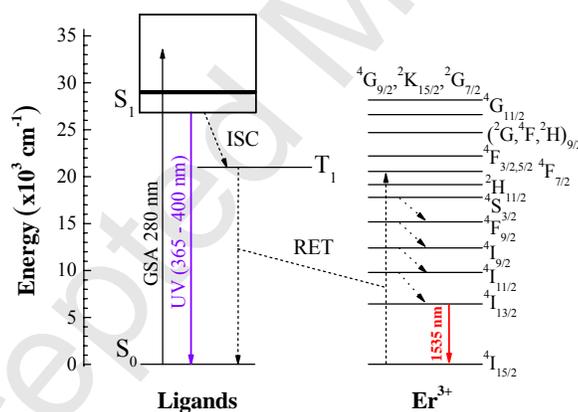


**Figure 11.** Scheme of the ground-state absorption (GSA), ligand-ligand intersystem crossing (ISC) processes, ligand-to-metal resonant energy transfer (RET) mechanisms, multiphonon de-excitations (---) and PL processes (in color). For clarity reasons the excited states of the three ligands were merged into one (for fod / bipy / bath, respectively: singlet ($^1\pi\pi^*$=35000 / 29900 / 29000 cm$^{-1}$) and triplet ($^3\pi\pi^*$=22500 / 22900 / 21000 cm$^{-1}$) [40-42]).

Upon excitation with a picosecond pulsed laser diode at 405 nm, the two complexes also show weak and broad emission in the visible range (see Figure 12). There are some dips in the emission spectra that can be readily associated to $Er^{3+}$ ions re-absorption. Similar effects are also present when the samples are excited with laser radiation at 470 nm (not shown). This re-absorption is a process in which a photon emitted by the ligand is absorbed by $Er^{3+}$ ions -which are not being excited directly by the laser- before leaving the sample. In order to observe this phenomenon, there must be a large overlap between the broad fluorescent emission band from the ligands and the absorption bands of the $Er^{3+}$ ions involved in the process (see the diffuse reflectance spectra of the complexes in Figure 9, also plotted in Figure 12 to allow direct comparison). The probability of these processes depends on how resonant these overlaps are,

12

although it also depends on the oscillator strength of the transitions involved. This accounts for the fact that the energy transfer between the ligands and the $Er^{3+}$ ions is more evident for transitions involving the $^2H_{11/2}$ upper level, since the $^4I_{15/2} \rightarrow {}^2H_{11/2}$ absorption peak has a larger experimental oscillator strength.



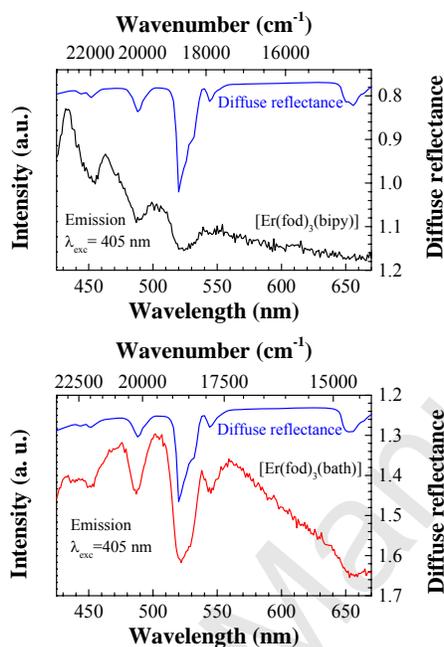**Figure 12.** Photoluminescence spectra in the visible region for the [Er(fod)$_3$(bipy)] (*black, top*) and [Er(fod)$_3$(bath)] (*red*, *bottom*) complexes upon excitation at 405 nm.

*PL emission in the C-band.* The NIR emission spectra for the two complexes were recorded using the $S_0 \rightarrow S_1$ excitation band maxima at 360 nm using a Xe lamp (see Figure 13). A broad emission in the near-IR region is obtained for both [Er(fod)$_3$(bipy)] and [Er(fod)$_3$(bath)] complexes, peaking at around 1530 nm. As mentioned above, such emission is the result of an efficient energy transfer from the organic ligands to the lanthanide ions in the resulting local environment in the complexes under study. This energy transfer by *antenna effect* is strongly influenced by the energy difference between the ligand triplet state and the levels of the lanthanide ion. In the case of $Er^{3+}$, there are resonant energy transfer channels from the ligands to the high energy states of the optically active ions, which decay by multiphonon relaxation to the $^4I_{13/2}$ metastable level, from which radiative relaxation to the ground state occurs by the NIR emission of light at around 1.53 µm.

Similar emission profiles have been found for the two complexes, with some structure associated to the Stark energy levels hyperfine structure and the electron population distributions of the $^4I_{13/2}$ and $^4I_{15/2}$ multiplets. The measurements of the NIR emission spectra upon direct excitation of the $^4I_{9/2}$ state at 800 nm with laser radiation yield the same results (not shown).

Since the two samples have been measured in the same conditions, a quantitative intensity comparison is applicable. The higher luminescence from the [Er(fod)$_3$(bath)] complex can be correlated with an improved energy transfer due its shorter Er-N distances [23] and to the bulkier and more rigid planar structure of bathophenanthroline [43,44,29,45].
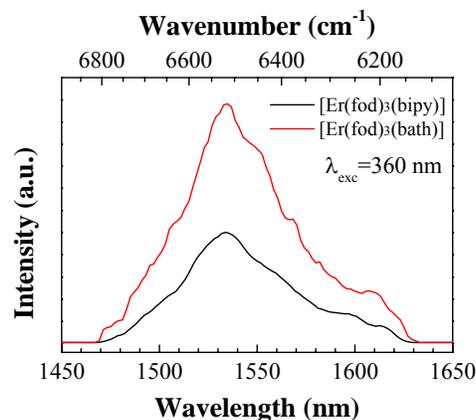
13

**Figure 13.** Photoluminescence spectra in the C-band upon ligand-mediated excitation in the UV region (λ=360 nm).

*Excitation spectra.* The excitation spectra of the complexes (monitored at the wavelength of interest, i.e., 1530 nm) feature an intense broad band between 300 and 400 nm with a maximum around 355-360 nm (see Figure 14). This band is attributed to ligand-centered ($S_0{\rightarrow}S_1$) transitions of *β*-diketonate and heterocyclic ligands [29,45], and the shift between UV-Vis absorption and excitation peaks is consistent with the literature (e.g. [46]). Thus, aforementioned *antenna effect* sensitization mechanism is further confirmed.
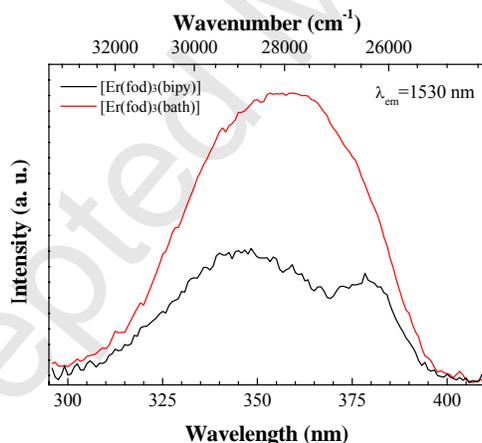


**Figure 14.** Excitation spectra under detection of the $Er^{3+}$ $^4I_{13/2}{\rightarrow}^4I_{15/2}$ emission at 1530 nm.

## 3.9. *Lifetime measurements*

The decay of the ligand fluorescence has been measured using a high repetition rate pulsed UV diode centered at 280 nm. The detection wavelength was tuned at the maximum of the $S_1{\rightarrow}S_0$ fluorescence band, at 370 for [Er(fod)$_3$(bipy)] and at 395 nm for [Er(fod)$_3$(bath)], respectively. The results are shown in Figure 15, where the instrument response function (IRF) that describes the temporal width of the pump pulses are also given (dotted lines). In the case of the [Er(fod)$_3$(bipy)] compound, the decay of the fluorescence is so fast that it cannot be resolved with this excitation source. For the [Er(fod)$_3$(bath)] complex, a longer and non-exponential decay is observed. The non-exponential character of the decay is characteristic of solid powder samples in which, in addition to the radiative and multiphonon relaxation processes, other interactions -such as ligand to ligand and ligand to metal interactions- contribute to the overall

14

decay of the fluorescence. In order to quantify the average lifetime value of the fluorescence, the decay curves have been successfully fitted to a double exponential decay of the type:

$$I(t) = B_1 \cdot e^{(-t/\tau_1)} + B_2 \cdot e^{(-t/\tau_2)} \qquad (1)$$

The fitting was made using IRF reconvolution analysis with F900 software (Edinburgh Instruments). The average lifetime is then calculated using the following equation [47]:

$$\tau_{av} = (B_1\tau_1^2 + B_2\tau_2^2)/(B_1\tau_1 + B_2\tau_2) \qquad (2)$$

The obtained average lifetime of the $S_1$ excited state of [Er(fod)$_3$(bath)] complex is about 2.72 ns. As noted above, the average lifetime of the ligand excited state of [Er(fod)$_3$(bipy)] cannot be determined using this fitting procedure because it is beyond the temporal resolution of the equipment, which is estimated to be about 0.5 ns. According to the excitation mechanism of the PL, there are several relaxation paths for the $S_1$ excited level of the ligand, namely, radiative, multiphonon, intersystem crossing, ligand to metal RET, or ligand to ligand ET processes. Taking into account that the excitation spectra show a higher ligand to metal RET efficiency for the [Er(fod)$_3$(bath)] complex, we tentatively propose that the shorter lifetime found for the [Er(fod)$_3$(bipy)] compound is an indication of higher probability of ligand relaxation due to vibrational modes of the surrounding environment, which would quench both its radiative emission as well as the ligand to metal RET probability.
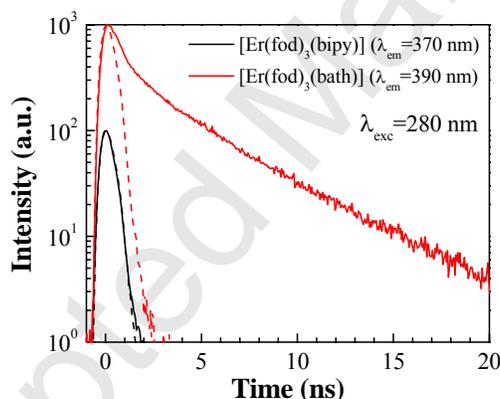


**Figure 15.** Decay of the fluorescence of [Er(fod)$_3$(bipy)] (*black*) and [Er(fod)$_3$(bath)] (*red*) complexes upon excitation at 280 nm and detection at the maximum of their emission bands. IRP (*dashed lines*) accounts for the instrument response function.

The NIR PL decay of the $^4I_{13/2}$ multiplet was measured after pumping at 980 nm with a MOPO laser at 10 Hz repetition rate. The decays show a single exponential behavior, which can be observed as a linear dependence in the semi-log representations of Figure 16. The good fitting to a single-exponential function confirms a unique and consistent coordination environment around the lanthanide ion [48]. The $^4I_{13/2}$ lifetimes obtained for the two complexes, namely $\tau$=1.503 and 1.394 μs for [Er(fod)$_3$(bipy)] and [Er(fod)$_3$(bath)], respectively, are quite similar between them and to other partly fluorinated Er$^{3+}$ $\beta$-diketonate complexes previously reported [49,50,21,23,26]. These values, although almost one order of magnitude larger than those reported for erbium(III) tris(8-hydroxyquinolate) or ErQ$_3$ (0.2 μs in powder form) [51], are significantly smaller than those attained for Er(F-tpip)$_3$ (where HF-tpip stands for tetrapentafluorophenylimidodiphosphinate) [52] or for perfluorinated nitrosopyrazolone-based erbium chelates [53]: 164 μs and 15.7 μs, respectively. Thus, it can be inferred that the fluorinated $\beta$-diketonate ligands need to be combined with perfluorinated N,N-donors so as to entirely eliminate the effect of the remaining C-H oscillators and further increase the lifetimes.
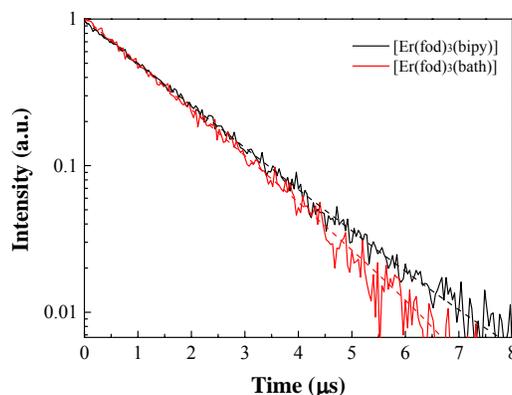
15

**Figure 16.** Room temperature PL decays of the $^4I_{13/2}$ multiplet measured under 980 nm excitation of $^4I_{11/2}$ $Er^{3+}$ level of the [Er(fod)$_3$(bipy)] (*black*) and [Er(fod)$_3$(bath)] (*red*) complexes. Single-exponential fits are also included (*dashed lines*).

## 4. Conclusion

In this work, we have successfully obtained two perfluorinated $Er^{3+}$ complexes with very low hydrogen content: elemental analysis confirmed that the percentage of hydrogen was between 3.16 and 3.29% and FTIR spectra do not show the deleterious high vibrational modes at 3500 cm$^{-1}$ that would appear if O-H bonds were present (only C-H vibrational modes at 3000-2500 cm$^{-1}$ as weak bands). On the other hand, the consistent octacoordination of the ligands chosen in the design of the complexes appears to be well suited for sensitizing the luminescence of the NIR-emitting $Er^{3+}$ ion, achieving an efficient energy transfer from the organic ligands (excited in the UV region) to the lanthanide ion in the resulting environment of [Er(fod)$_3$(N,N-donor)] complexes. The higher luminescence from the [Er(fod)$_3$(bath)] complex has been correlated with an improved energy transfer due to the bulkier and more rigid planar structure of bathophenanthroline and shorter Er-N distances. Moreover, the quenching of the organic ligands emission reinforces the hypothesis that the new ternary complexes display a favored photoluminescence in the C-band that makes them promising materials for erbium-doped waveguides, NIR-OLEDs or other optoelectronic devices.

Finally, it is also noteworthy that semi-empirical quantum chemistry methods –and in particular the novel Sparkle/PM7– have proven to be a very suitable approach for conducting an *educated-guess* when dealing with incomplete structural data, since these methods are not only substantially faster than *ab initio* ones, but can model large unit cells (2048 atoms) with remarkable accuracy.

## Acknowledgments

16

**Supplementary data**
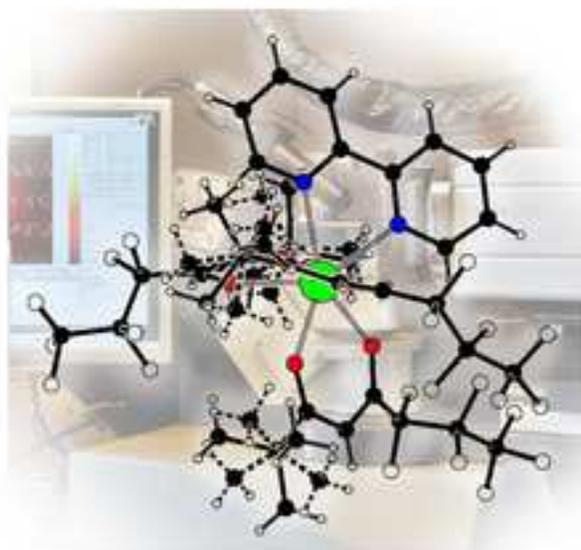
CCDC 1005117 contains the supplementary crystallographic data for [Er(fod)₃(bipy)]. These data can be obtained free of charge via http://www.ccdc.cam.ac.uk/conts/retrieving.html, or from the Cambridge Crystallographic Data Centre, 12 Union Road, Cambridge CB2 1EZ, UK; fax: (+44) 1223-336-033; or e-mail: deposit@ccdc.cam.ac.uk.
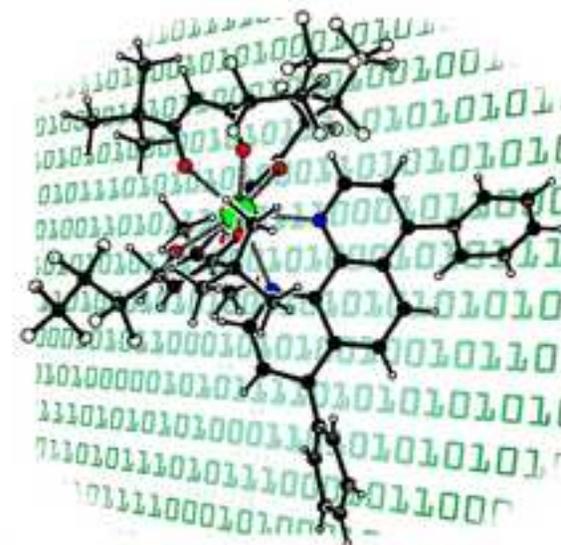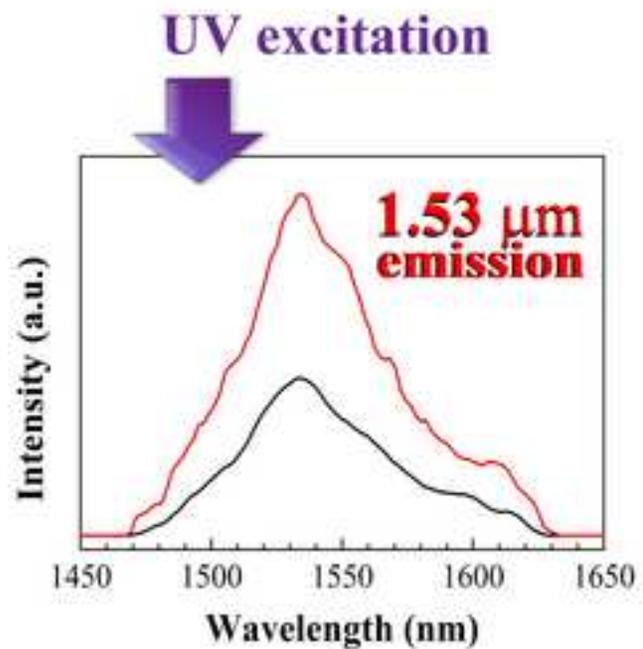
**References**

[1] Ye, H. Q., Z. Li, Y. Peng, C. C. Wang, T. Y. Li, Y. X. Zheng, A. Sapelkin, G. Adamopoulos, I. Hernández, P. B. Wyatt and W. P. Gillin (2014) Organo-erbium systems for optical amplification at telecommunications wavelengths. *Nature Materials* **13,** 382-386.

[2] Lehn, J.-M. (1990) Perspectives in Supramolecular Chemistry—From Molecular Recognition towards Molecular Information Processing and Self-Organization. *Angewandte Chemie International Edition in English* **29,** 1304-1319.

[3] Sabbatini, N., M. Guardigli and J.-M. Lehn (1993) Luminescent lanthanide complexes as photochemical supramolecular devices. *Coord. Chem. Rev.* **123,** 201-228.

[4] de Sá, G. F., O. L. Malta, C. de Mello Donegá, A. M. Simas, R. L. Longo, P. A. Santa-Cruz and E. F. da Silva (2000) Spectroscopic properties and design of highly luminescent lanthanide coordination complexes. *Coord. Chem. Rev.* **196,** 165-195.

[5] Tan, R. H. C., M. Motevalli, I. Abrahams, P. B. Wyatt and W. P. Gillin (2006) Quenching of IR Luminescence of Erbium, Neodymium, and Ytterbium β-Diketonate Complexes by Ligand C−H and C−D Bonds. *The Journal of Physical Chemistry B* **110,** 24476-24479.

[6] Monguzzi, A., R. Tubino, F. Meinardi, A. O. Biroli, M. Pizzotti, F. Demartin, F. Quochi, F. Cordella and M. A. Loi (2009) Novel Er3+Perfluorinated Complexes for Broadband Sensitized Near Infrared Emission. *Chem. Mater.* **21,** 128-135.

[7] Pietrantoni, S., R. Francini, R. Pizzoferrato, S. Penna, R. Paolesse and F. Mandoj (2007) Energy transfer and excitation processes in thin films of rare-earth organic complexes for NIR emission. *physica status solidi (c)* **4,** 1048-1051.

[8] Pizzoferrato, R., R. Francini, S. Pietrantoni, R. Paolesse, F. Mandoj, A. Monguzzi and F. Meinardi (2010) Effects of Progressive Halogen Substitution on the Photoluminescence Properties of an Erbium−Porphyrin Complex. *The Journal of Physical Chemistry A* **114,** 4163-4168.

[9] Van Deun, R., P. Fias, P. Nockemann, A. Schepers, T. N. Parac-Vogt, K. Van Hecke, L. Van Meervelt and K. Binnemans (2004) Rare-Earth Quinolinates: Infrared-Emitting Molecular Materials with a Rich Structural Chemistry. *Inorg. Chem.* **43,** 8461-8469.

[10] Van Deun, R., P. Fias, K. Driesen, K. Binnemans and C. Görller-Walrand (2003) Halogen substitution as an efficient tool to increase the near-infrared photoluminescence intensity of erbium(iii) quinolinates in non-deuterated DMSO. *PCCP* **5,** 2754.

[11] Sheldrick, G. (1996) SADABS. University of Göttingen, Göttingen, Germany.

[12] Sheldrick, G. M. (2007) A short history ofSHELX. *Acta Crystallographica Section A Foundations of Crystallography* **64,** 112-122.

[13] Spek, A. L. (2003) Single-crystal structure validation with the programPLATON. *J. Appl. Crystallogr.* **36,** 7-13.

[14] Maia, J. D. C., G. A. Urquiza Carvalho, C. P. Mangueira, S. R. Santana, L. A. F. Cabral and G. B. Rocha (2012) GPU Linear Algebra Libraries and GPGPU Programming for Accelerating MOPAC Semiempirical Quantum Chemistry Calculations. *Journal of Chemical Theory and Computation* **8,** 3072-3081.

[15] Stewart, J. J. P. (2012) MOPAC2012. Stewart Computational Chemistry, Colorado Springs, CO, USA.

[16] Dutra, J. D. L., M. A. M. Filho, G. B. Rocha, R. O. Freire, A. M. Simas and J. J. P. Stewart (2013) Sparkle/PM7 Lanthanide Parameters for the Modeling of Complexes and Materials. *Journal of Chemical Theory and Computation* **9,** 3333-3341.

[17] Stewart, J. J. P. (2012) Optimization of parameters for semiempirical methods VI: more modifications to the NDDO approximations and re-optimization of parameters. *J. Mol. Model.* **19,** 1-32.

[18] Stewart, J. J. P. (2007) Optimization of parameters for semiempirical methods V: Modification of NDDO approximations and application to 70 elements. *J. Mol. Model.* **13,** 1173-1213.

[19] Freire, R. O. and A. M. Simas (2010) Sparkle/PM6 Parameters for all Lanthanide Trications from La(III) to Lu(III). *Journal of Chemical Theory and Computation* **6,** 2019-2023.

17

[20] Orpen, A. G., L. Brammer, F. H. Allen, O. Kennard, D. G. Watson and R. Taylor (1989) Supplement. Tables of bond lengths determined by X-ray and neutron diffraction. Part 2. Organometallic compounds and co-ordination complexes of the d- and f-block metals. *J. Chem. Soc., Dalton Trans.*, S1.

[21] Martín-Ramos, P., V. Lavín, M. Ramos Silva, I. R. Martín, F. Lahoz, P. Chamorro-Posada, J. A. Paixão and J. Martín-Gil (2013) Novel erbium(III) complexes with 2,6-dimethyl-3,5-heptanedione and different N,N-donor ligands for ormosil and PMMA matrices doping. *Journal of Materials Chemistry C* **1,** 5701.

[22] Martín-Ramos, P., M. Ramos Silva, J. T. Coutinho, L. C. J. Pereira, P. Chamorro-Posada and J. Martín-Gil (2014) Single-Ion Magnetism in a Luminescent Er3+ β-Diketonato Complex with Multiple Relaxation Mechanisms. *Eur. J. Inorg. Chem.* **2014,** 511-517.

[23] Martín-Ramos, P., M. R. Silva, C. Coya, C. Zaldo, Á. L. Álvarez, S. Álvarez-García, A. M. Matos Beja and J. Martín-Gil (2013) Novel erbium(III) fluorinated β-diketonate complexes with N,N-donors for optoelectronics: from synthesis to solution-processed devices. *Journal of Materials Chemistry C* **1,** 2725.

[24] Ramos Silva, M., P. Martín-Ramos, J. T. Coutinho, L. C. J. Pereira and J. Martín-Gil (2014) Effect of the capping ligand on luminescent erbium(iii) β-diketonate single-ion magnets. *Dalton Transactions* **43,** 6752.

[25] Martín-Ramos, P., P. S. Pereira da Silva, V. Lavín, I. R. Martín, F. Lahoz, P. Chamorro-Posada, M. Ramos Silva and J. Martín-Gil (2013) Structure and NIR-luminescence of ytterbium(III) beta-diketonate complexes with 5-nitro-1,10-phenanthroline ancillary ligand: assessment of chain length and fluorination impact. *Dalton Transactions* **42,** 13516.

[26] Martín-Ramos, P., C. Coya, Á. L. Álvarez, M. Ramos Silva, C. Zaldo, J. A. Paixão, P. Chamorro-Posada and J. Martín-Gil (2013) Charge Transport and Sensitized 1.5 μm Electroluminescence Properties of Full Solution-Processed NIR-OLED based on Novel Er(III) Fluorinated β-Diketonate Ternary Complex. *The Journal of Physical Chemistry C* **117,** 10020-10030.

[27] Irfanullah, M. and K. Iftikhar (2010) New hetero-dilanthanide complexes containing Ln1(fod)3 and Ln2(fod)3 fragments (Ln=Pr–Nd; Nd–Sm; Eu–Tb and Ho–Er) linked by bis-diimine bridging ligand. *Inorg. Chem. Commun.* **13,** 694-698.

[28] Irfanullah, M. and K. Iftikhar (2009) New dinuclear lanthanide(III) complexes based on 6,6,7,7,8,8,8-heptafluoro-2,2-dimethyl-3,5-octanedione and 2,2′-bipyrimidine. *Inorg. Chem. Commun.* **12,** 296-299.

[29] Irfanullah, M. and K. Iftikhar (2010) Photoluminescence, optical absorption and hypersensitivity in mono- and dinuclear lanthanide (TbIII and HoIII) β-diketonate complexes with diimines and bis-diimine bridging ligand. *J. Lumin.* **130,** 1983-1993.

[30] Gerasimova, T. P. and S. A. Katsyuba (2013) Bipyridine and phenanthroline IR-spectral bands as indicators of metal spin state in hexacoordinated complexes of Fe(ii), Ni(ii) and Co(ii). *Dalton Transactions* **42,** 1787.

[31] Tayyari, S. F., M. Vakili, A.-R. Nekoei, H. Rahemi and Y. A. Wang (2007) Vibrational assignment and structure of trifluorobenzoylacetone. *Spectrochimica Acta Part A: Molecular and Biomolecular Spectroscopy* **66,** 626-636.

[32] Liang, C. F., E. J. Schmitschek and J. A. Trias (1970) I.R. and Raman spectra of europium(III) β-diketonates. *J. Inorg. Nucl. Chem.* **32,** 811-831.

[33] Irfanullah, M. and K. Iftikhar (2013) Synthesis and spectroscopic analysis of an extended series of hetero dinuclear complexes containing two different lanthanides in 1:1 stoichiometry. *Inorg. Chim. Acta* **394,** 373-384.

[34] Villata, L. S., E. Wolcan, M. R. Féliz and A. L. Capparelli (1998) Solvent quenching of the 5D0 → 7F2 emission of Eu(6,6,7,7,8,8,8-heptafluoro-2,2-dimethyl-3,5-octanedionate)3. *Journal of Photochemistry and Photobiology A: Chemistry* **115,** 185-189.

[35] Gerasimova, V. I. (2005) Optical Spectroscopy of the Eu(FOD)[sub 3] Complex Impregnated into the Free Volume of Nanoporous Glass and Polymethylmethacrylate Using Supercritical Carbon Dioxide. *Opt. Spectrosc.* **98,** 564.

[36] Gerasimova, V. I., Y. S. Zavorotny, A. O. Rybaltovskii, A. A. Antoshkov, V. I. Sokolov, E. V. Troitskaya and V. N. Bagratashvili (2011) Modification of the optical properties of fluoropolymers by supercritical fluid impregnation with europium β-diketonates. *Russian Journal of Physical Chemistry B* **4,** 1149-1157.

[37] Gerasimova, V. I., A. A. Antoshkov, Y. S. Zavorotny, A. O. Rybaltovskii and D. A. Lemenovskii (2013) Optical properties of europium(III) β-diketonate/polymer-doped systems using supercritical carbon dioxide. *J. Lumin.* **134,** 339-344.

18

[38] Görller-Walrand, C. and K. Binnemans (1998) Spectral intensities of f-f transitions. In *Handbook on the physics and chemistry of rare earths*, Vol. 25. (Edited by K. A. Gschneidner and L. Eyring ), pp. 101-264. Elsevier BV, Amsterdam.

[39] Irfanullah, M. and K. Iftikhar (2011) A comparative study of 1H NMR and sensitized visible light emission of an extended series of dinuclear lanthanide complexes. *Journal of Photochemistry and Photobiology A: Chemistry* **224,** 91-101.

[40] Voloshin, A. I., N. M. Shavaleev and V. P. Kazakov (2001) Luminescence of praseodymium (III) chelates from two excited states (3P0 and 1D2) and its dependence on ligand triplet state energy. *J. Lumin.* **93,** 199-204.

[41] Raj, D. B. A., S. Biju and M. L. P. Reddy (2008) One-, Two-, and Three-Dimensional Arrays of Eu3+-4,4,5,5,5-pentafluoro-1-(naphthalen-2-yl)pentane-1,3-dione complexes: Synthesis, Crystal Structure and Photophysical Properties. *Inorg. Chem.* **47,** 8091-8100.

[42] Ambili Raj, D. B., S. Biju and M. L. P. Reddy (2009) Highly luminescent europium(iii) complexes containing organosilyl 4,4,5,5,5-pentafluoro-1-(naphthalen-2-yl)pentane-1,3-dionate ligands grafted on silica nanoparticles. *J. Mater. Chem.* **19,** 7976.

[43] Yang, X.-D., W.-B. Chang and Y.-X. Ci (1994) Time-resolved fluorescence immunoassay with measurement of a europium chelate in solution: dissociation conditions and application for determination of cortisol. *Anal. Chem.* **66,** 2590-2594.

[44] Yang, Y. S., M. L. Gong, Y. Y. Li, H. Y. Lei and S. L. Wu (1994) Effects of the structure of ligands and their Ln3+ complexes on the luminescence of the central Ln3+ ions. *J. Alloys Compd.* **207-208,** 112-114.

[45] Irfanullah, M. and K. Iftikhar (2010) Hypersensitivity in the Luminescence and 4f–4f Absorption Properties of Mono- and Dinuclear EuIII and ErIII Complexes Based on Fluorinated β-Diketone and Diimine/ Bis-Diimine Ligands. *Journal of Fluorescence* **21,** 81-93.

[46] Kokuoz, B., J. R. DiMaio, C. J. Kucera, D. D. Evanoff and J. Ballato (2008) Color Kinetic Nanoparticles. *J. Am. Chem. Soc.* **130,** 12222-12223.

[47] Lakowicz, J. R. (2006) *Principles of fluorescence spectroscopy.* Springer, New York.

[48] Gago, S., J. A. Fernandes, J. P. Rainho, R. A. Sá Ferreira, M. Pillinger, A. A. Valente, T. M. Santos, L. D. Carlos, P. J. A. Ribeiro-Claro and I. S. Gonçalves (2005) Highly Luminescent Tris(β-diketonate)europium(III) Complexes Immobilized in a Functionalized Mesoporous Silica. *Chem. Mater.* **17,** 5077-5084.

[49] Li, Z., J. Yu, L. Zhou, H. Zhang, R. Deng and Z. Guo (2008) 1.54μm Near-infrared photoluminescent and electroluminescent properties of a new Erbium (III) organic complex. *Org. Electron.* **9,** 487-494.

[50] Li, X., Z. Si, C. Pan, L. Zhou, Z. Li, X. Li, J. Tang and H. Zhang (2009) Near-infrared luminescent properties and natural lifetime calculation of a novel Er3+ complex. *Inorg. Chem. Commun.* **12,** 675-677.

[51] Magennis, S. W., A. J. Ferguson, T. Bryden, T. S. Jones, A. Beeby and I. D. W. Samuel (2003) Time-dependence of erbium(III) tris(8-hydroxyquinolate) near-infrared photoluminescence: implications for organic light-emitting diode efficiency. *Synth. Met.* **138,** 463-469.

[52] Mancino, G., A. J. Ferguson, A. Beeby, N. J. Long and T. S. Jones (2005) Dramatic Increases in the Lifetime of the Er3+Ion in a Molecular Complex Using a Perfluorinated Imidodiphosphinate Sensitizing Ligand. *J. Am. Chem. Soc.* **127,** 524-525.

[53] Beverina, L., M. Crippa, M. Sassi, A. Monguzzi, F. Meinardi, R. Tubino and G. A. Pagani (2009) Perfluorinated nitrosopyrazolone-based erbium chelates: a new efficient solution processable NIR emitter. *Chem. Commun.*, 5103.

19

X-ray diffraction

UV excitation

1.53 µm emission

Intensity (a.u.)

1450 1500 1550 1600 1650
Wavelength (nm)

Sparkle/PM7